Optics Letters

On the origin of the optical vortex lattices in a nematic liquid crystal light valve

Enrique Calisto,[1,2] Marcel G. Clerc,[2,*] Michał Kowalczyk,[1] and Panayotis Smyrnelis[3]

[1]Departamento de Física and Millennium Institute for Research in Optics, Facultad de Ciencias Físicas y Matemáticas, Universidad de Chile, Casilla 487-3, Santiago, Chile
[2]Departamento de Ingeniería Matemática and CMM, Universidad de Chile, Casilla 170 Correo 3, Santiago, Chile
[3]Institute of Mathematics, Polish Academy of Sciences, 00-656 Warsaw, Poland
*Corresponding author: marcel@dfi.uchile.cl

Received 29 January 2019; revised 7 May 2019; accepted 9 May 2019; posted 13 May 2019 (Doc. ID 359005); published 3 June 2019

Optical vortices and lattices of these are attracting the attention of the scientific community because of their applications in various fields of optical processing, communications, enhanced imaging systems, and bio-inspired devices. Programmable optical vortices lattices with arbitrary distributions have been achieved using illuminated liquid crystals with photosensitive walls. Using an amplitude equation that describes these optical valves close to the Freédericksz transition allows us to characterize analytically the vortices and the lattices they form. The numerical simulations of the amplitude equation, analytical solutions, and experimental observations show good agreement.

https://doi.org/10.1364/OL.44.002947

Optical vortices are point phase dislocations; that is, they are singular points where the electromagnetic field goes to zero and around which the phase distribution forms an N-armed spiral, with N being the topological charge [1–3]. In the last decade, optical vortices have attracted attention for their diverse photonic applications [4], ranging from the interchange of angular momentum between light and matter [5], optical tweezers [6–8], quantum computation [9], enhancement of astronomical images [10], the generation of optical beams by micro/nano patterned in liquid crystals [11–16], and data transmission [17]. In all these applications, optical vortex lattices are always involved and required, because they contain multiple optical vortices that supply information, flexibility, and manipulation [17–19]. Indeed, the generation, detection, and manipulation of optical vortex lattices are of fundamental relevance in the research described and in future optical applications. The realization of programable lattices of optical vortices with arbitrary distribution in space was demonstrated by exploiting reorientational nonlinearities in the nematic liquid crystal layer of a light valve [20]. The vortex arrangements were determined qualitatively on the basis of consistent topological rules governing light-induced matter defects of both signs. When a liquid crystal light valve is illuminated by a Gaussian beam, a vortex in the molecular orientation (umbilic defect) is induced [21,22]. The umbilical defects are topological charges ± 1.

In this Letter, we establish analytically the origin of the vortex lattices observed in illuminated liquid crystal layers with photosensitive walls. Using a topologically driven Ginzburg–Landau equation that describes illuminated liquid crystal light valves close to the Fréedericksz transition, we model the vortices and the lattices they form. Figure 1 shows typical experimental, numerical, and analytical vortex lattices of an illuminated liquid crystal light valve. The numerical simulations of the amplitude equation, analytical solutions, and experimental observations show good agreement.

The liquid crystal light valve is composed of a thin nematic liquid crystal film sandwiched between a glass and a photoconductive plate. The liquid crystal light valve is filled with a nematic mixture exhibiting negative dielectric anisotropy. The transparent interfaces are treated in order to provide a homeotropic alignment of the liquid crystals, that is, close to the walls, the liquid crystal molecules are perpendicular to the confining layers, one of which is the photoconductive slab. The director $\vec{n}(z,x,y,t)$ accounts for the orientational organization of the molecules, where z and $\{x,y\}$, respectively, are the longitudinal and transverse coordinates. Owing to the photoconductive substrate and transparent electrodes, when the liquid crystal light valve is illuminated, the effective voltages $V(z,x,y)$ drop across the liquid crystal layer which acquires a profile proportional to the light intensity $I(x,y)$ on the liquid crystal layer, $V(z,x,y) = z/d[V_0 + \alpha I(x,y)]$ [21]. Where V_0 is the voltage applied to the liquid crystal light valve, d and α are the thickness of the valve and the phenomenological dimensional parameter, respectively, that describe the linear response of the photoconductor.

The elongated molecules of the liquid crystal start to reorient as a result of the torque exerted by the induced electric field and tend to align perpendicularly to it. The homeotropic state, $\vec{n} = \hat{z}$, undergoes an stationary instability for a critical voltage. Indeed, this molecular reorientation instability corresponds to the Fréedericksz transition [23]. Close to this transition, one can use the following ansatz for the amplitude of the critical spatial mode $\vec{n} \approx [u(x,y,t)\sin(\pi z/d), v(x,y,t)\sin(\pi z/d), 1 - (u^2+v^2)\sin^2(\pi z/d)/2]$. Substituting it in the director

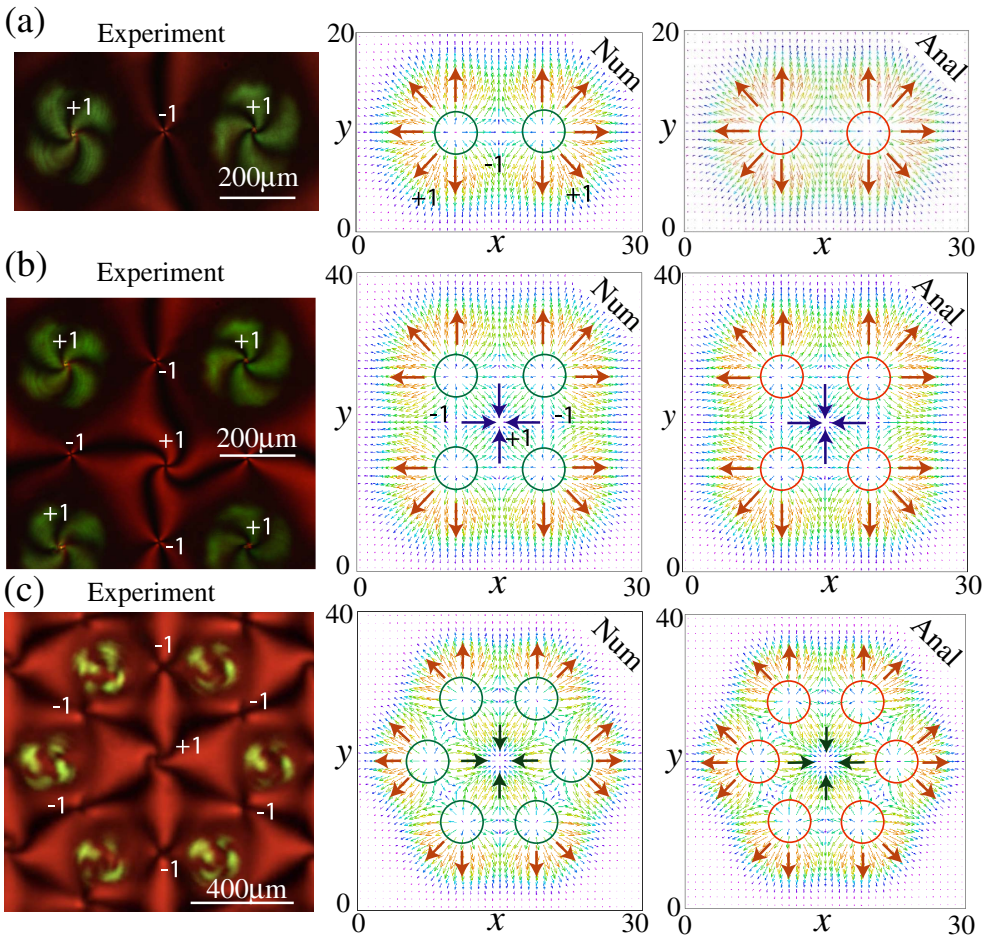

Fig. 1. Optical vortex lattices in nematic liquid crystals. The left panels correspond to snapshots of vortex lattices obtained in an illuminated nematic liquid crystal light valve with (a) two, (b) four, and (c) six light beams (courtesy of R. Barboza). The ±1 account for the respective topological charges. The intermediate panels correspond to the numerical simulations of the topological driven Ginzburg–Landau Eq. (1) with $\mu = -3$, $a = 1$, $\delta = 0$, and $b = 0.1$, forced, respectively with (a) two, (b) four, and (c) six Gaussians beams. The right panels correspond to analytical vortex lattices obtained using formula $A = -4b\nabla_{r_\perp}\langle V\rangle/\alpha$ with (a) two, (b) four, and (c) six Gaussians beams. The circles account for the waist of the respective Gaussian beams.

equation—which contains the effects of elasticity and electromagnetic couplings—integrating in z coordinate over the sample thickness and, considering the complex amplitude $A \equiv (u + iv)$, after straightforward calculations, one obtains the topologically driven Ginzburg–Landau equation [20,21]

$$\gamma\partial_t A = \mu A - aA|A|^2 + \nabla_\perp^2 A + \delta\partial_{\eta\eta}\bar{A} + bI' e^{i\theta}, \quad \textbf{(1)}$$

where $\mu(r) \equiv -K_3(\pi/d)^2 - \epsilon_a(V_0 + \alpha I)^2/d^2$ is the bifurcation parameter; $a \equiv -[K_3(\pi/d)^2/4 + 3\epsilon_a(V_0 + \alpha I)^2/4d^2] > 0$ is the nonlinear response; $b \equiv 2\epsilon_a d\alpha V_0/\pi$, $\partial_\eta \equiv \partial_x + i\partial_y$, and $\delta \equiv (K_1 - K_2)/(K_1 + K_2)$ stand for the anisotropy elasticity of the system; θ is the amplitude phase; $I' \equiv \sqrt{(\partial_x I)^2 + (\partial_y I)^2}$; γ is the rotational viscosity; and $\{K_1, K_2, K_3\}$ are the elastic anisotropy constants of the liquid crystal.

The numerical simulations of the amplitude Eq. (1) with a forcing term consisting of a superposition of Gaussians equivalent to illuminating the optical valve with several light beams give vortex lattices as a stable equilibrium. The middle panels of Fig. 1 show the typical lattices. Circles account for the waist of the Gaussian forcing. When the liquid crystal light valve is forced with a single beam of sufficiently intense light, it always induces a vortex of positive charge at the center of the beam [22]. This result is easily understood as a consequence of the voltage induced by a single ray being an electric field with a positively charged vortex [21]. Figure 1 shows the vortices induced by a green laser. Illuminating the sample with a red laser, we analyze other areas of response of the optical valve. In the case of two light beams, the positive charges must be accompanied by negative charges, since the total topological charge must be conserved. To characterize analytically the origin of these vortices we assume $\mu < 0$ (i.e., we are below the Fréedericksz transition) and consider a single ray of light with intensity $I = I_0 e^{-r_\perp^2/w^2}$, where I_0 and w, respectively, are the strength and waist of the light beam, and $r_\perp = \sqrt{x^2 + y^2}$ is the radial coordinate with its origin in the center of the beam. When $w \gg 1$, Eq. (1) has the following approximate stationary solution:

$$A_R(r_\perp, \phi) = -\frac{bI'(x,y)}{\mu} e^{i\phi} = \frac{2bI_0}{w^2\mu} r_\perp e^{-r_\perp^2/w^2} e^{i\phi}, \quad \textbf{(2)}$$

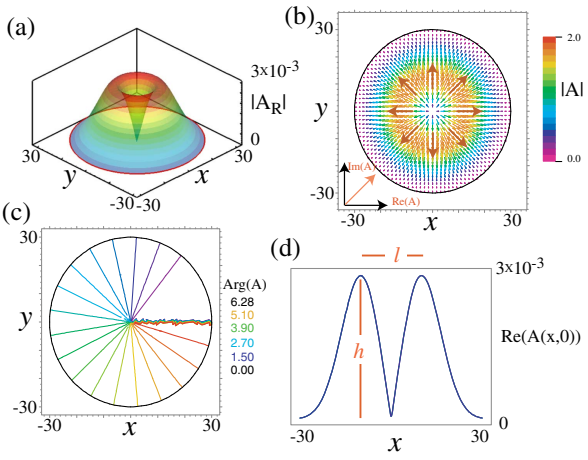

Fig. 2. Rayleigh vortex of the topologically driven Ginzburg–Landau equation (1) with $\mu = -3$, $a = 1$, $\delta = 0$, $b = 1$, $I_0 = 0.01$, and $w = 30$. (a) Surface plot of the Rayleigh vortex, Eq. (2). (b) Vector representation of the vortex solution. The colors show the magnitude of the amplitude $|A|$. (c) Counter-plot of the phase of amplitude A, $\arg(A) = \mathrm{Im}(A)/\mathrm{Re}(A)$. (d) Rayleigh vortex profile; h and l account for the height and width of the core of the vortex, respectively.

where ϕ is the angular coordinate with its origin in the center of the Gaussian. It can be checked that the error of this approximate solution is of the order $O(\frac{1}{w^6})$; in other words, both the nonlinear term and the Laplacian are negligible in this limit. Since $A_R(r_\perp, \phi)$ grows linearly around the origin and decays as a Gaussian, we have called this solution a *Rayleigh vortex*. Figure 2 show the surface plot, vectorial representation, and phase of the Rayleigh vortex. The maximum value h that the vortex reaches corresponds to vortex height, $h = 2bI_0/\mu w\sqrt{2e}$, and the width of the vortex core is $l = w/\sqrt{2}$. Figure 3 shows a comparison between the numerical solutions of the topologically driven Ginzburg–Landau equation (1) and the approximate solution (2). From this figure, we infer that for the light beam of the big waist, the Rayleigh vortex is is a very good approximation of the topologically driven Ginzburg–Landau vortex. For light beam waists of the order one, the effect of the Laplacian and the nonlinear term begins to play a role, and the Rayleigh solution ceases to be dominant. Experimentally, the standard width used for the waist of the light beam (250 μm) is 50 times larger than the length associated with the elastic constant (5 μm), that is, in our dimensionless units $w = 50$. Then, below the Fréedericksz transition, the Rayleigh vortex describes the umbilical defects.

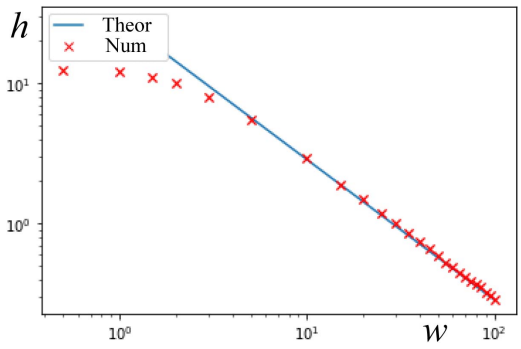

Fig. 3. Log-log plot of the height of the vortex as a function of beam waist w. The heights obtained by numerical simulation of the topologically forced Ginzburg–Landau Eq. (1) (crosses) with $\mu = -3$, $a = 1$, $\delta = 0$, $b = 1$, and $I_0 = 0.01$ are compared with $h = 2bI_0/\mu w\sqrt{2e}$ (continuous line).

To explain the origin of Rayleigh vortex, we note that the liquid crystal light valve is a thin film and, thus, one should consider averaged quantities. The voltage averaged over the thickness $\langle V(r_\perp)\rangle$ takes the form

$$\langle V(r_\perp)\rangle = \frac{1}{d}\int_0^d V(z, r_\perp)\mathrm{d}z = \frac{V_0 + \alpha I(r_\perp)}{2}. \quad \textbf{(3)}$$

Likewise, calculating the electric field averaged in the vertical direction, we obtain $\langle E(r_\perp, \phi)\rangle = -\nabla_{r_\perp}\langle V\rangle = \alpha I_0(r_\perp/2w^2)e^{-r_\perp^2/w^2}e^{i\phi}$, where the electric vector is represented in complex variable notation. Therefore, the Rayleigh vortex is proportional to the averaged electric field or, equivalently the gradient of the averaged potential $A_R(r_\perp, \phi) = 4b\langle E\rangle/\alpha = -4b\nabla_{r_\perp}\langle V\rangle/\alpha$.

Generalizing the previous analysis, one can consider two light beams illuminating the optical light valve in different positions (r_1 and r_2). The averaged potential $\langle V(r_\perp)\rangle = (V_0 + \alpha I(x, y, r_1) + \alpha I(x, y, r_2))/2$, where $I(x, y, r_i)$ is a Gaussian beam centered at r_i, corresponds to a surface with two mounds. Since the equilibrium amplitude is the gradient of the averaged potential, we identify maxima or minima of the potential with positively charged vortices and the saddle points with vortices of negative charge. Figure 4 illustrates this in the case of two Gaussian beams. Note that a negative vortex is located between the positive vortices. By decreasing the

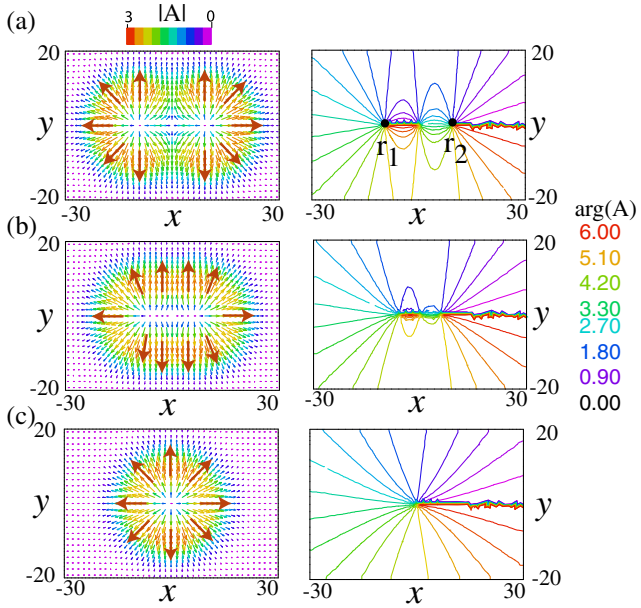

Fig. 4. Analytical vortices induced by two Gaussians. The total topological charge is $N = 1$. The complex amplitude A was obtained using formula $A = -4b\nabla_{r_\perp}\langle V\rangle/\alpha$. The left panels correspond to the vector representation of the complex amplitude. The colors account for the magnitude of the amplitude. The contour plot of the phase of the amplitude is shown on the left panel. (a), (b), and (c) correspond to Gaussians with different distances.

distance between the centers of the Gaussians, the charges approach each other [see Fig. 4(b)]. When this distance is of the order of the beam waist, the vortices merge, leaving a single vortex of positive charge [see Fig. 4(c)]. Based on the same strategy, one can build configurations with more Gaussian beams using the formula $A = -4b\nabla_{r_\perp}\langle V\rangle/\alpha$. Figure 1 (right panels) shows vortex lattices obtained by superposing two, four, and six equally spaced Gaussian beams. An excellent agreement is observed with the vortex lattices obtained by numerical simulations of the topologically driven Ginzburg–Landau equation (1). Likewise, there is excellent agreement with the experimental observations. However, due to the anisotropic effects that are not accounted for in the Rayleigh vortex approximation, the experimental positive vortices exhibit swirling arms [24]. Note that in the case of four light beams, the averaged potential has four saddle points on the sides of the square formed by the maxima and a minimum on the intersection of the diagonals. This explains why in the experiment a swirling vortex is induced on the diagonal between the topologically forced vortices [see the left panels of Figs. 1(b) and 1(c)].

In conclusion, we have been able to establish analytically the origin of the vortex lattices observed in illuminated liquid crystal layers with photosensitive walls below the Fréedericksz transition. The numerical simulations of the amplitude equation, analytical solutions, and experimental observations show good agreement. When the system is above the molecular reorientation transition, the elastic couplings (taken into account in (1) by the Laplacian and the second-order differential operator describing anisotropic spatial variations with $\delta \neq 0$) determine the vortex core size, which is now of the order of few microns. In this regime, the Rayleigh vortex does not account for the observed vortices. However, the position and configuration of the vortex lattices are qualitatively described by the lattices of the Rayleigh vortices. The amplitude equations describe qualitatively and quantitatively the dynamics near the instability point. However, these equations qualitatively describe the dynamics away from the bifurcation point [2,25]. Hence, analytically presented findings are valid far from the Fréedericksz transition.

At the onset of the Fréedericksz transition, depending on the light intensity, the vortices positioned in the center of the light beam can undergo instabilities and move to dark areas (the area outside the illuminated region). These new topological defects known as the *shadow vortices* [26] are characterized by having an exponentially small height. Experimentally they are detected indirectly. The lattice created by these and the induced vortices is a problem currently in progress.

Funding. Millennium Institute for Research in Optics; Fondecyt (1130126, 1170164, 1180903, 3160055); CONICYT Becas Magister Nacional 2017 (22171924); Fondo Basal CMM-Chile (AFB170001); Narodowe Centrum Nauki (NCN) (2017/26/E/ST1/00817).

Acknowledgment. The authors thank R. Barboza, C. Castillo, V. Zambra, and M. Ferre for fruitful discussions. E. Calisto acknowledges the financial support of CONICYT through Becas Magister Nacional 2017. M. Kowalczyk was partially supported by Chilean research grants Fondecyt and Fondo Basal CMM-Chile. P. Smyrnelis was partially supported by Fondo Basal CMM-Chile, Fondecyt postdoctoral, and the National Science Centre, Poland.

REFERENCES

1. J. F. Nye and M. V. Berry, Proc. R. Soc. London A **336**, 165 (1974).
2. L. M. Pismen, *Vortices in Nonlinear Fields* (Oxford Science, 1999).
3. M. S. Soskin and M. V. Vasnetov, *Progress in Optics*, E. Wolf, ed. (Elsevier, 2001), Vol. **42**, p. 219.
4. A. S. Desyatnikov, Y. S. Kivshar, and L. Torner, *Progress in Optics*, E. Wolf, ed. (Elsevier, 2005), Vol. **47**, p. 291.
5. L. Allen, M. W. Beijersbergen, R. J. C. Spreeuw, and J. P. Woerdman, Phys. Rev. A **45**, 8185 (1992).
6. D. G. Grier, Nature **424**, 810 (2003).
7. V. G. Shvedov, A. V. Rode, Y. V. Izdebskaya, A. S. Desyatnikov, W. Krolikowski, and Y. S. Kivshar, Phys. Rev. Lett. **105**, 118103 (2010).
8. M. Padgett and R. Bowman, Nat. Photonics **5**, 343 (2011).
9. H. H. Arnaut and G. A. Barbosa, Phys. Rev. Lett. **85**, 286 (2000).
10. F. Tamburini, G. Anzolin, G. Umbriaco, A. Bianchini, and C. Barbieri, Phys. Rev. Lett. **97**, 163903 (2006).
11. Z. G. Zheng, C. L. Yuan, W. Hu, H. K. Bisoyi, M. J. Tang, Z. Liu, P. Z. Sun, W. Q. Yang, X. Q. Wang, D. Shen, Y. Li, F. Ye, Y. Q. Lu, G. Li, and Q. Li, Adv. Mater. **29**, 1703165 (2017).
12. P. Chen, L. L. Ma, W. Duan, J. Chen, S. J. Ge, Z. H. Zhu, M. J. Tang, R. Xu, W. Gao, T. Li, W. Hu, and Y. Q. Lu, Adv. Mater. **30**, 1705865 (2018).
13. B. Y. Wei, W. Hu, Y. Ming, F. Xu, S. Rubin, J. G. Wang, V. Chigrinov, and Y. Q. Lu, Adv. Mater. **26**, 1590 (2013).
14. B. Y. Wei, S. Liu, P. Chen, S. X. Qi, Y. Zhang, W. Hu, Y. Q. Lu, and J. L. Zhao, Appl. Phys. Lett. **112**, 121101 (2018).
15. P. Chen, S. J. Ge, L. L. Ma, W. Hu, V. Chigrinov, and Y. Q. Lu, Phys. Rev. Appl. **5**, 044009 (2016).
16. P. Chen, S. J. Ge, W. Duan, B. Y. Wei, G. X. Cui, W. Hu, and Y. Q. Lu, ACS Photonics **4**, 1333 (2017).
17. J. Wang, J.-Y. Yang, I. M. Fazal, N. Ahmed, Y. Yan, H. Huang, Y. Ren, Y. Yue, S. Dolinar, M. Tur, and A. E. Willner, Nat. Photonics **6**, 488 (2012).
18. T. Lei, M. Zhang, Y. R. Li, P. Jia, G. N. Liu, X. G. Xu, Z. H. Li, C. J. Min, J. Lin, C. Y. Yu, H. B. Niu, and X. C. Yuan, Light Sci. Appl. **4**, e257 (2015).
19. L. Stoyanov, G. Maleshkov, M. Zhekova, I. Stefanov, D. N. Neshev, G. G. Paulus, and A. Dreischuh, J. Opt. Soc. Am. B **35**, 402 (2018).
20. R. Barboza, U. Bortolozzo, G. Assanto, E. Vidal-Henriquez, M. G. Clerc, and S. Residori, Phys. Rev. Lett. **111**, 093902 (2013).
21. R. Barboza, U. Bortolozzo, M. G. Clerc, S. Residori, and E. Vidal-Henriquez, Adv. Opt. Photonics **7**, 635 (2015).
22. R. Barboza, U. Bortolozzo, G. Assanto, E. Vidal-Henriquez, M. G. Clerc, and S. Residori, Phys. Rev. Lett. **109**, 143901 (2012).
23. V. Freedericksz and V. Zolina, Trans. Faraday Soc. **29**, 919 (1927).
24. R. Barboza, U. Bortolozzo, S. Residori, M. G. Clerc, and E. Vidal-Henriquez, Philos. Trans. R. Soc. A. **372**, 20140019 (2014).
25. M. C. Cross and P. C. Hohenberg, Rev. Mod. Phys. **65**, 851 (1993).
26. R. Barboza, U. Bortolozzo, M. G. Clerc, J. D. Davila, M. Kowalczyk, S. Residori, and E. Vidal-Henriquez, Phys. Rev. E **93**, 050201 (2016).